World Scientific
www.worldscientific.com

Optimization for the Harvesting Structure of the Piezoelectric Bimorph Energy Harvesters Circular Plate by Reduced Order Finite Element Analysis

A. N. Solovyev[*,†,‡] and L. V. Duong[§,¶]

*Department of Theoretical and Applied Mechanics
Don State Technical University, Rostov on Don, Russia*

†*Department of Mathematics, Mechanics and Computer Sciences
Southern Federal University
Rostov on Don, Russia*

‡*Department of Mechanics of Active Materials
Southern Scientific Centre of Russian Academy of Sciences
Rostov on Don, Russia*

§*Department of Vehicle Engineering
Le Quy Don Technical University, Ha Noi, Vietnam*
¶*leduong145@gmail.com*

The power generation efficiency of piezoelectric energy harvesters is dependent on the coupling of their resonant frequency with that of the source vibration. The mechanical design of the energy harvester plays an important role in defining the resonant frequency characteristics of the system and therefore in order to maximize power density, it is important for a designer to be able to model, simulate and optimize designs to match new target applications. This paper gives a detailed calculation of piezoelectric energy harvesters that is in the form of a bimorph-circular plate fixed in the contour in the device frame by finite element (FE) analysis using the commercially available software package ANSYS, ACELAN. The piezoelectric bimorph is assumed to be driven into flexural vibration by an ambient acoustic source to convert the mechanical energies into electric energies. The optimal design was based on matching the resonant frequency of the device with the environmental exciting frequency, and balancing the output voltage. The simplified models of the account of a proof mass are offered. On the basis of calculations, the most effective construction of the device is offered that exhibit the targeted resonant frequency response chosen by the designer.

Keywords: Finite element (FE); piezoelectric generator (PEG); optimization; bimorph; circular plate; resonant frequency.

¶Corresponding author.

1. Introduction

The energy from piezoelectric devices is an alternate power source, which allows agglomerating energy from low radiant powers in a surrounding medium, for example, vibration from oscillating bridges, vehicles, etc. [Ali and Adhikari, 2013; Boisseau *et al.*, 2013; Xie *et al.*, 2014]. The strain-rate dependent charge output of piezoelectric materials has typically been used for sensor applications and can be found in a variety of different devices including accelerometers, microphones, load cells, etc. [Sodano *et al.*, 2005; Kobayashi *et al.*, 2010; Zhang *et al.*, 2013b]. Recently, energy storage devices in particular piezoelectric are widely studied. There are several excellent and comprehensive survey papers and monographs, notably Sodano *et al.* [2004b], Anton and Sodano [2007], Priya [2007], Tang *et al.* [2010], Priya and Inman [2009] and Erturk and Inman [2011b], reviewing the state of the art in different time phases of investigations related to piezoelectric energy harvesting.

Piezoelectric power generators have many advantages over other conversion methods. Piezoelectric generators (PEGs) consist of piezoelectric ceramics, and electrodes which cover them. Because of their simplicity, PEGs can even be made on the scale of micro–electro–mechanical systems. Another advantage is that the lifetime of the system is almost unlimited if the applied force and external temperature are within the operational range. Unlike the power generation methods that rely on heat conversion, a PEG presents no problems, such as heat isolation. For comprehensive reviews of its literature, we refer the reader to Erturk and Inman [2011a], Stanton *et al.* [2012], Monri and Maruo [2013], Farnsworth *et al.* [2014], Gafforelli *et al.* [2015], Jung *et al.* [2015].

Of the published results that focus on the piezoelectric effect as the transduction method, almost all have focused on harvesting by using cantilever beams with one piezoceramic layer or two piezoceramic layers [Litak *et al.*, 2010; Staaf *et al.*, 2015; Fan *et al.*, 2015]. The exceptions are, Kim *et al.* [2005a, 2005b] presented a theoretical analysis and experimental verification of a clamped unimorph piezoelectric plate structure that was then used to study the effect of geometric parameters and electrode configuration so that the factors that lead to maximum electrical energy generation in relation to a given volume of material or applied mechanical force, pressure, or stress are determined. Adhikari *et al.* [2009] developed a stack configuration and harvesting broadband vibration energy, a more practically available ambient source.

Ali and Adhikari [2013] analyzed the prospect of using a vibration absorber for possible energy harvesting: a vibration absorber is supplemented with a piezoelectric stack for both vibration confinement and energy harvesting. Mehmood *et al.* [2013] investigated the concept of harvesting energy from a circular cylinder undergoing vortex-induced vibrations. A thermal energy harvester using piezo-shaped memory alloy composite, was designed by Namli and Taya [2011]. The main mechanism of such a piezo-shaped memory alloy composite is the synergistic effect of piezoelectrics and shape memory alloy, which are connected in series and subjected to

fluctuating temperature. Boisseau *et al.* [2013] analyzed a resonance phenomenon that enables an increase of vibration energy harvesters of output power (compared to non-resonant systems), by using nonlinear springs. The influence on the plate's overall properties resulted from the surface elasticity and piezoelectricity of piezoelectric bimorph nano-actuators is modeled by a spring force exerting on the boundary of the bulk core [Zhang *et al.*, 2013a]. The free and forced vibration characteristics of a functionally graded piezoelectric materials beam under thermo–electro–mechanical loads using third-order shear deformation beam theory was presented by Doroushi *et al.* [2011]. Lezgy-Nazargah *et al.* [2013] developed an FE modeling for static and dynamic analyses of functionally graded piezoelectric beams. Experimental efforts to validate analytically predicted energy generating performance of piezoelectric circular diaphragms for use in a pressure-loaded system was presented by Mo *et al.* [2010].

There have been many applications of piezoelectric energy harvesting [Anton and Sodano, 2007; Kim *et al.*, 2011], however the development of theoretical models to predict the electromechanical response is equally important for advancement of this field. The majority of the models have been based on a single-degree-of-freedom spring mass [Dutoit *et al.*, 2005; Jeon *et al.*, 2005; Roundy *et al.*, 2005; Twiefel *et al.*, 2008]. In this approach, the beam is modeled by a second-order ordinary differential equation with the beam tip displacement as its dependent variable. For increasing the accuracy of the solution, Sodano *et al.* [2004a] applied the Rayleigh–Ritz method to describe the energy harvesting as a summation of continuous mode shapes. Erturk and Inman [2008] later found a closed form solution for the energy harvesting. More recently, Liao and Sodano [2008] modified the model of Sodano *et al.* [2004a] to allow for an efficient study of the power harvesting system, and optimal parameters could be identified. Vatanabe *et al.* [2013] used topology optimization and homogenization to design functionally graded piezocomposite materials for utilizing at energy harvesting applications. Amini *et al.* [2014] developed an FE model for investigating homogenous piezoelectric energy harvesters. This model can be used for varying cross-sectional area and also for different base excitations and loads.

In this article, the investigations of circular plate elements are carried out to analyze their suitability for piezoelectric energy generation. The structure has a substrate, which is glued between two piezoceramic plates. The harvester is equipped with a proof mass on the upper surface of the piezoelectric element, which can be tuned so that the fundamental natural frequency of the PEG is close to a dominant excitation frequency available in the ambient vibration-energy spectrum. The cross-section of bimorph PEG circular plate is shown in Fig. 1. The interest here is in determining the factors that lead to maximum electrical energy generation in relation to a given volume of material or dimensions of the PEG (Fig. 1). The ANSYS and ACELAN FE modeling software was used for this task.
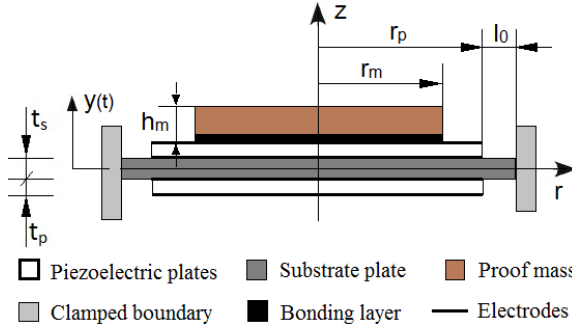
Fig. 1.   Cross-section of bimorph PEG circular plate.

2. Continual and Finite Element Problem Statements

2.1. *Continual statement of problem of the electric elasticity*

In finite-element packages ANSYS and ACELAN, the Rayleigh method is used as a rule, to take account of the attenuation in composite, solid structures. We will now extend the Rayleigh method for taking account of attenuation, which has been described above, to structures containing elastic and piezoelectric media. In the case of piezoelectric media $\Omega_j = \Omega_{pk}$, we shall assume that the mechanical stress tensor $\boldsymbol{\sigma}$ and the electric induction vector $\mathbf{D}$ are related to the deformation tensor $\boldsymbol{\varepsilon}$ and the electric field strength vector $\mathbf{E}$ by the equations

$$\boldsymbol{\sigma} = \boldsymbol{c}_j^E \cdot (\boldsymbol{\varepsilon} + \beta_{dj}\dot{\boldsymbol{\varepsilon}}) - \boldsymbol{e}_j^T \cdot \mathbf{E}; \quad \mathbf{D} + \varsigma_d\dot{\mathbf{D}} = \mathbf{e}_j \cdot (\boldsymbol{\varepsilon} + \varsigma_d\dot{\boldsymbol{\varepsilon}}) + \mathfrak{z}_j^S \cdot \mathbf{E}, \tag{1}$$

where c_j^E are the components of the elastic constant tensor; e_j is piezoelectric stress coefficients; $\mathfrak{z}_j^S$ are the components of the dielectric permittivity tensor. (For elastic media $\Omega_j = \Omega_{ek}$ the piezomodules e_j are equal to zero).

We shall assume that a piezoelectric device is a solid Ω consisting of N homogeneous domains Ω_j ($j = 1, 2, \ldots, N$), generally speaking, with different piezoelectric or elastic properties. We shall assume that, in the domains $\Omega_j = \Omega_{pk}$ with piezoelectric properties, the displacement vector $\mathbf{u}(x, t)$ and the electric potential $\phi(x, t)$ satisfy the system of equations ($\mathbf{f}_j$ is the mass force density vector)

$$\rho_j\ddot{\mathbf{u}} + \alpha_{dj}\rho_j\dot{\mathbf{u}} - \nabla \cdot \boldsymbol{\sigma} = \mathbf{f}_j; \quad \nabla \cdot \mathbf{D} = 0, \tag{2}$$

for the governing relations (1.1), (1.2) and the formulae

$$\boldsymbol{\varepsilon} = (\nabla\mathbf{u} + \nabla\mathbf{u}^T)/2, \quad \mathbf{E} = -\nabla\phi, \tag{3}$$

where ρ_j is the continuous function of coordinates (density); $\alpha_{dj}, \beta_{dj}, \zeta_d$ are the nonnegative damping coefficients, and the other symbols are the standard designations for theory of electroelasticity with the exception of index "j", corresponding for area Ω_j.

For the media $\Omega_j = \Omega_{ek}$ with pure elastic properties, only stress fields would be considered. Similarly Eqs. (1)–(3) and constitutive relationships are used with

negative electric fields and piezoelectrical connectivity effects. Equations (1)–(3) are added to the mechanical and electrical boundary conditions, as well as the initial conditions in the case of non-stationary problem.

In particular, for electrode (S_e) included in external circuit, besides a condition of constancy of the electric potential, which in this case is to be an unknown function, it is added the condition defining electric current flowing through this electrode:

$$\int_{S_e} \dot{D}_n ds = I, \tag{4}$$

where I — the current of the circuit, which is in the case of free electrode, equals zero; D_n — the normal component of the vector of the electric induction.

2.2. *Finite element approach*

We use FE modeling in classic Lagrangian formulation to solve dynamic problems of acoustic electric elasticity. We choose coherent FE mesh specified in the areas Ω_{hj}, which approach area Ω_j. There are unknown field functions $\mathbf{u}$, ϕ and ψ in this mesh. We approximate them as

$$\mathbf{u}(\mathbf{x}, t) = \mathbf{N}_u^T(\mathbf{x}) \cdot \mathbf{U}(t), \quad \phi(\mathbf{x}, t) = \mathbf{N}_\phi^T \cdot \mathbf{\Phi}(t), \quad \psi(\mathbf{x}, t) = \mathbf{N}_\psi^T(\mathbf{x}) \cdot \mathbf{\Psi}(t); \tag{5}$$

where $\mathbf{N}_u$ is the shape function matrix for displacement field $\mathbf{u}$; $\mathbf{N}_\varphi$ and $\mathbf{N}_\psi$ are the shape vector-functions for the electric potential fields ϕ and speed potential in acoustic medium ψ, respectively; and $\mathbf{U}(t)$, $\mathbf{\Phi}(t)$, $\mathbf{\Psi}(t)$ are the global vectors of the corresponding nodal degrees of freedom.

FE modeling approximation (5) of the generalized formulations of dynamic problems (1) – (3), including principal and natural boundary conditions, results in the following system of differential equations:

$$\mathbf{M} \cdot \ddot{\mathbf{a}} + \mathbf{C} \cdot \dot{\mathbf{a}} + \mathbf{K} \cdot \mathbf{a} = \mathbf{F}. \tag{6}$$

$$\mathbf{M} = \begin{pmatrix} \mathbf{M}_{uu} & 0 & \tilde{\mathbf{R}}_{u\psi} \\ 0 & 0 & 0 \\ \tilde{\mathbf{R}}_{u\psi}^T & 0 & -\mathbf{M}_{\psi\psi} \end{pmatrix}, \quad \mathbf{C} = \begin{pmatrix} \mathbf{C}_{uu} & 0 & \mathbf{R}_{u\psi} \\ \varsigma_d \mathbf{K}_{u\phi}^T & 0 & 0 \\ \mathbf{R}_{u\psi}^T & 0 & -\mathbf{C}_{\psi\psi} \end{pmatrix},$$

$$\mathbf{K} = \begin{pmatrix} \mathbf{K}_{uu} & \mathbf{K}_{u\phi} & 0 \\ \mathbf{K}_{u\phi}^T & -\mathbf{K}_{\phi\phi} & 0 \\ 0 & 0 & -\mathbf{K}_{\psi\psi} \end{pmatrix}, \quad \mathbf{F} = \left\{ \begin{array}{c} \mathbf{F}_u \\ \mathbf{F}_\phi + \varsigma_d \dot{\mathbf{F}}_\phi \\ 0 \end{array} \right\}, \tag{7}$$

relatively of the vector of unknown $\mathbf{a} = [\mathbf{U}, \; \mathbf{\Phi}, \; \mathbf{\Psi}]^T$. Here $\mathbf{C}_{uu} = \Sigma_j(\alpha_{dj}\mathbf{M}_{uuj} + \beta_{dj}\mathbf{K}_{uuj})$, where $\mathbf{M}_{uuj}$ and $\mathbf{K}_{uuj}$ are the structural FE of mass and stiffness matrix. Other elements of the submatrix (6), (7) are described in Belokon *et al.* [2002].

The FE modeling equation system for *eigenvalue (eigenfrequency)* problems has the following form:

$$-\omega^2 \mathbf{M} \cdot a + \mathbf{K} \cdot a = 0. \tag{8}$$

$$\mathbf{M} = \begin{pmatrix} \mathbf{M}_{uu} & 0 \\ 0 & 0 \end{pmatrix}, \quad \mathbf{K} = \begin{pmatrix} \mathbf{K}_{uu} & \mathbf{K}_{u\phi} \\ \mathbf{K}_{u\phi}^T & -\mathbf{K}_{\phi\phi} \end{pmatrix}. \tag{9}$$

Steady-state vibration problems arise, when $\mathbf{F}_u = \tilde{\mathbf{F}}_u(\mathbf{x}) \exp(j\omega t), \mathbf{F}_\phi = \tilde{\mathbf{F}}_\phi(\mathbf{x}) \exp(j\omega t)$, $\mathbf{a} = \tilde{\mathbf{a}}(\mathbf{x}) \exp(j\omega t)$. It is easy to derive a system of linear algebraic equations from (6), (7) relatively of the amplitude vector $\tilde{\mathbf{a}}$ in the form:

$$\mathbf{K}_c \cdot \tilde{\mathbf{a}} = \tilde{\mathbf{F}}_c, \quad \tilde{\mathbf{F}}_c = \left[\tilde{\mathbf{F}}_u, \tilde{\mathbf{F}}_\phi, 0 \right]^T. \tag{10}$$

$$\mathbf{K}_c = \begin{pmatrix} \mathbf{K}_{uuc} & \mathbf{K}_{u\phi} & \mathbf{K}_{u\psi c} \\ \mathbf{K}_{u\phi}^T & -\mathbf{K}_{\phi\phi c} & 0 \\ \mathbf{K}_{u\psi c}^T & 0 & -\mathbf{K}_{\psi\psi c} \end{pmatrix}. \tag{11}$$

$$\mathbf{K}_{\eta\eta c} = -\omega^2 \mathbf{M}_{\eta\eta} + i\omega\, \mathbf{C}_{\eta\eta} + \mathbf{K}_{\eta\eta}, \quad \eta = u, \psi. \tag{12}$$

$$\mathbf{K}_{u\psi c} = -\omega^2 \tilde{\mathbf{R}}_{u\psi} + i\omega\, \mathbf{R}_{u\psi}, \quad \mathbf{K}_{\phi\phi c} = \frac{1}{(1 + i\omega\zeta_d)} \mathbf{K}_{\phi\phi}. \tag{13}$$

3. Analytical Modeling and Optimization of the PEG

3.1. *Axi-symmetric model*

The device modeled is a bimorph with an internal steel substrate and two thin layers of piezoceramic PZT-4 on either sides, a proof mass on the upper surface of the piezoelectric element. Aluminum, Steel or Lead was used as the material of the proof mass. Thus, it can easily realize low resonant frequency corresponding to most vibration sources in our living environment as well as the vibration frequency (for example, $100\,\text{Hz}$), at which this research is aimed. Advocating for their outside diameter substrate plate clamped along the contour of the base of the case. The dimensions of the constituents are selected based on the approximate guideline of PEG design. The thickness of the PZT-4 t_p and the radius r_p; the thickness of the substrate plate t_s and the radius $r_s = r_p + l_0 (l_0 = 2\,\text{mm}$ — constant); the height of proof mass h_m and the radius r_m (Fig. 1). The material properties of piezoceramic PZT-4 are given in Table 1 [Berlincourt *et al.*, 1964]; Aluminum, Steel and Lead are given in Table 2.

The β_{dj} parameter (Eqs. (1)–(13)) was calculated from the tabulated mechanical quality factor Q_m and the resonant frequency of the device: $\beta_{dj} = 1/\omega Q_m$.

The clamped edges of the PEG is subjected to a harmonic displacement:

$$y(t) = y_0 e^{-i(2\pi f)t}, \tag{14}$$

where $y_0 = 0.1\,\text{mm}$ — is the amplitude oscillation, f is the oscillation frequency.

Table 1.   Material properties of piezoceramic PZT-4 (used in the FE-calculation)[a].

c_{11}^E (GPa)	c_{12}^E (Gpa)	c_{13}^E (GPa)	c_{33}^E (GPa)	c_{44}^E (GPa)	e_{31} (C/m^2)	e_{33} (C/m^2)	e_{15} (C/m^2)	$\varepsilon_{31}/\varepsilon_0$	$\varepsilon_{33}/\varepsilon_0$
139	77.8	77.4	115	25.6	-5.2	15.1	12.7	730	635

Note: [a]$\varepsilon_0 = 8.85 \times 10^{-12}$ C^2/Nm^2 — permittivity of free space, $\rho = 7.5 \times 10^3$ kg/m^3 — density, $Q_m = 100$ — quality factor.

Table 2.   Properties of construction materials (used in the FE-calculation).

	Density (kg/m^3)	Young's modulus (GPa)	Poisson's ratio	Quality factor, Q_m
Steel	7800	210	0.3	2500
Lead	11340	16	0.42	2500
Aluminum	2700	68	0.36	2500

Because the PEG exhibits axi-symmetry about its central axis, it was modeled as a two-dimensional axi-symmetric body. A two-dimensional axi-symmetric model offers the advantage over the corresponding three-dimensional model in that the size of the model is smaller and consequently calculation time is much lesser. In packages ANSYS and ACELAN, the FE models of the considered devices are constructed by using axi-symmetric FE PLANE13 and PLANE42 based on a precise statement of the problems (1)–(13).

Next, we study the characteristics of the PEG at the influence harmonically varying during vibration on it and discuss ways to optimize the construction. In the paper, the achievement of the highest output voltage values is produced by changing the height and the type of material of the proof mass, thickness t_p, t_s and dimensions r_m, r_p.

3.2. *Calculation model of the PEG*

In this section, three models of the piezoelectric bimorph energy harvesters circular plate are investigated. The first harvester lacks bonding layer between the proof mass and the piezoceramic layer (the model with the proof mass rigidly attached on the piezoceramic layer), the second harvester considers the presence of the bonding layer (the model that is between the proof mass and the piezoceramic layer containing with bonding layer without interfering greatly bending the bimorph (Fig. 1), in the third harvester, the account of proof mass is constructed by using the boundary condition on the front surface of the upper piezoelectric layer, which has the form:

$$\sigma_z = M\omega^2(u_z + y_0)/S, \quad \tau_{zr} = 0 \quad \text{at } z = h_m, \tag{15}$$

where M is the inertial mass, ω is the circular frequency of vibrations, S is the square of upper site of the piezoelement to which is fixed the proof mass.
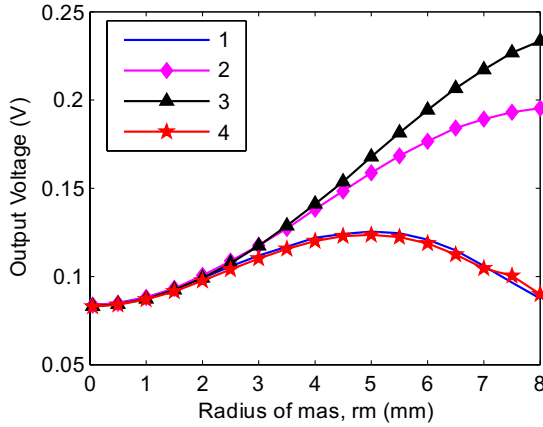
Fig. 2. The dependence of the output voltage on the radius of the proof mass r_m. 1 — the first harvester (ACELAN), 2 — the second harvester (ACELAN), 3 — the third harvester (ACELAN), 4 — the first harvester (ANSYS).

A PEG with $t_p = 0.5\,\text{mm}$, $r_p = 8\,\text{mm}$, $t_s = 0.5\,\text{mm}$, $r_s = 10\,\text{mm}$, $h_m = 2\,\text{mm}$, and r_m was changing from 0 to 8 mm, the material of the proof mass — lead is modeled to comparing the efficiency of three models. We investigate the dependence of the output voltage on the free electrode depending on the radius of the proof mass for the three harvesters for frequency vibration 100 Hz. The results are presented in Fig. 2.

From Fig. 2, it is followed that the results for the first harvester in case using packages ACELAN (curve 1) and ANSYS (curve 4) show good agreement for the entire range of the radius of the proof mass.

In cases where the calculations were carried out in packages ACELAN for the three harvesters (curve 1, 2 and 3) obviously, with the condition that the radius of the proof mass $r_m \leq 1.5\,\text{mm}$, the value of the output voltage of the three harvesters are similar. If value of the radius of the proof mass $1.5\,\text{mm} \leq r_m \leq 3.5\,\text{mm}$, the value of the output voltage for the second harvester (curve 2) and the third harvester (curve 3) are similar, but they are more than the value of the output voltage for the first harvester (curve 1). If the value of the radius of the proof mass $r_m \geq 3.5\,\text{mm}$, the value of the output voltage for the second harvester (curve 2) is higher than the output voltage for the first harvester (curve 1), but lower than the output voltage of the third harvester (curve 3). The value of the output voltage to the second harvester and the third harvester becomes larger and continues to increase monotonically, whereas, for the first harvester with $r_m = 5\,\text{mm}$ it reached the maximum (stiffness of the flywheel effect on the deflection of the bimorph). As it can be seen, by increasing the value of the radius of the proof mass r_m, we increase the value of the output voltage difference for the second and the third harvester, due to the influence of the stiffness of the bonding layer.

Our calculations show that the results from the second and third harvesters are approximately coincided, especially, for the lower range of relative radius of proof mass.

Thus, the model of PEG that is between the proof mass and the piezoceramic layer containing with bonding layer without interfering greatly bending the bimorph (the second harvester) is the most effective. Furthermore, they reduce the stress concentration at connection surface of piezoelectric and non-piezoelectric layers.

3.3. *Construction optimization*

There are key factors that we need to consider during the optimization design of the PEG — the resonant frequency, the output voltage density, which will be elaborated in this section.

Following is the rational choice (output voltage attains maximum) of the parameter values r_m, r_p, t_p, t_s, h_m, and the type of material of the proof mass for the second harvester (Fig. 1), which has proof mass, is divided by the bonding layer with a piezoceramic layer. We set the vibration frequency of the external load at 100 Hz, typical for vibrating machinery.

3.3.1. *Analysis on the resonant frequency of the PEG*

The resonant frequency of the piezoelectric energy converter is one of the most important factors influencing the converting efficiency of a device from mechanical energy to electrical energy. It must be designed to match the environmental vibration frequency, which is the prerequisite to maximize the output power.

The resonant frequency of the PEG was primarily analyzed to design the piezoelectric power generator with the wanted resonant frequency, since the maximum power (generated or converted) can only be achieved when the resonant frequency of the generator is matching the frequency of the vibration source.

Parameter designs of PEG were considered to calculate the resonant frequencies using FE package ANSYS, ACELAN. The targeted resonant frequency was attained by changing the radius and thickness of the piezoelectric plate and the metal plate, the height and radius of the proof mass and the type of material of the proof mass.

Let us consider the impact on the resonant frequency of the thickness t_s and t_p, radius r_m and r_p, height h_m and the type of material of the proof mass. The obtained dependences are shown in Figs. 3–5.

For the first plot, Fig. 3, it shows the relationship between the resonant frequency and the radius of the piezoelectric plate and the radius of the proof mass, where r_m was changing from 1 mm to 25 mm; $l_p = r_p - r_m$ was changing from 1 mm to 30 mm; the thickness of the substrate plate $t_s = 0.12$ mm; the thickness of the PZT-4 $t_p = 0.127$ mm, which are the typical values measured from commercial PZT plates and disks (Piezo System Co.); the height of the proof mass $h_m = 7$ mm, and the lead was selected as the proof mass because of its high density, which
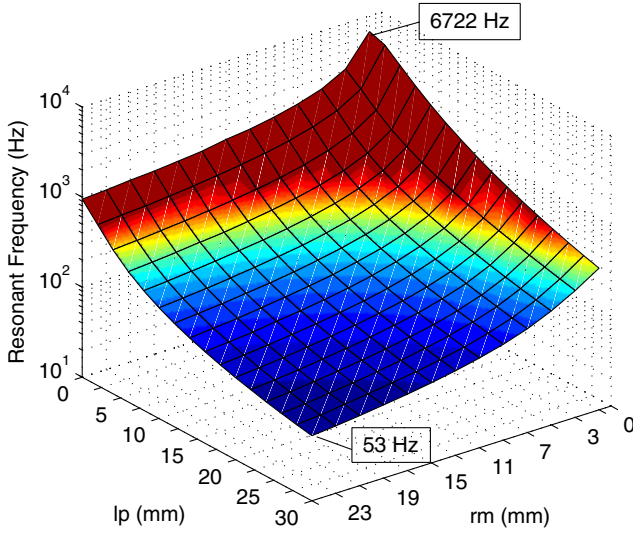
Fig. 3.　The dependence of the resonant frequency on the dimensions r_m and $l_p = r_p - r_m$.
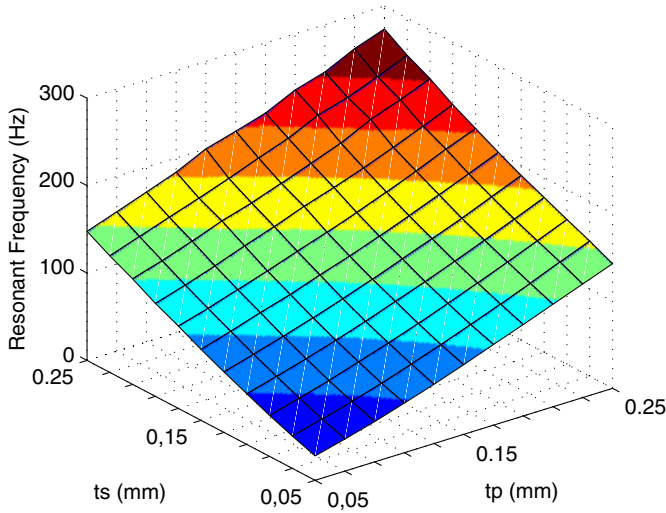

Fig. 4.　The dependence of the resonant frequency on the thickness t_s, t_p.

is $\rho_m = 11340\,\text{kg/m}^3$. All parameter values were selected according to the wanted resonant frequency, $100\,\text{Hz}$. In the case, when the frequency of the forced vibration is fixed (for example, $100\,\text{Hz}$), the built surface to determine the range of the geometric parameters r_m, r_p and in which the frequency is resonant.

For the second plot, Fig. 4, it shows the relationship between the resonant frequency and the thickness of the piezoelectric plate t_p and the thickness of the
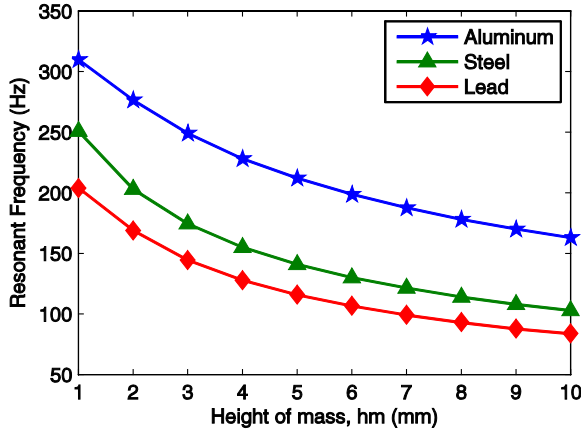
Fig. 5.   The dependence of the resonant frequency on the height of the proof mass h_m.

substrate plate t_s, where $r_p = 38$ mm; $r_m = 18$ mm; t_p was changing from 0.05 mm to 0.25 mm, t_s was changing from 0.05 mm to 0.25 mm; the height of the inertial element $h_m = 7$ mm and the material of the proof mass — lead. All parameter values were also selected according to the wanted resonant frequency, 100 Hz.

For the third plot, Fig. 5, it shows the relationship between the resonant frequency and the height of the proof mass h_m and the type of material of the proof mass (aluminum, steel, lead), where $r_m = 18$ mm, $r_p = 38$ mm, $t_p = 0.127$ mm, $t_s = 0.12$ mm; h_m was changing from 1 mm to 10 mm. All parameter values were again selected according to the wanted resonant frequency, 100 Hz.

From these three plots, it is verified that the resonant frequency decreases with increasing both the radius of the piezoelectric plate and the proof mass, decreases with decreasing both thicknesses of the piezoelectric plate and the substrate plate, and decreases with increasing the height of the proof mass.

These simulations helped us to design the optimal dimensions of PEG with wanted resonant frequency after considering together with the simulations of output power and safety issues. According to data presented in Figs. 3–5, it may be selected parameters of the device to work effectively in the frequency range between 30 Hz and 10000 Hz, where $l_p = r_p - r_m$, was changing from 1 mm to 30 mm; r_m was changing from 1 mm to 25 mm; t_s was changing from 0.05 mm to 0.25 mm; t_p was changing from 0.05 mm to 0.25 mm; h_m was changing from 1 mm to 10 mm.

Thus, the obtained results can select the optimum size of PEG with the necessary resonant frequency. In particular, if the frequency of forced vibration is 100 Hz, the rational geometric dimensions of construction positioned in the range: r_p was changing from 38 mm to 40 mm, $t_s + t_p$ was changing from 0.23 mm to 0.25 mm, h_m was changing from 6 mm to 7 mm and the material of the proof mass — lead, the PEG works effectively for the forced vibration frequency of 100 Hz.

3.3.2. *Analysis on the output voltage of the PEG*

In this section, we find the dependence of the output voltage on the free electrode depending on the thickness t_s and t_p, the radius r_m and r_p, the height of the proof mass h_m and the type of material of the proof mass. The values $r_p = 38$ mm and $t_s + t_p = 0.24$ mm are constant; the values r_m was changing from 5 mm to 37 mm; t_s was changing from 0.05 mm to 0.18 mm; h_m was changing from 1 mm to 10 mm. We set the vibration frequency of the external load at 100 Hz, typical for vibrating machinery, the results presented in Figs. 6 and 7.

Thus, Fig. 6 shows the dependence of the values of the output voltage on the free electrode depending on the radius of the proof mass r_m and thickness of the
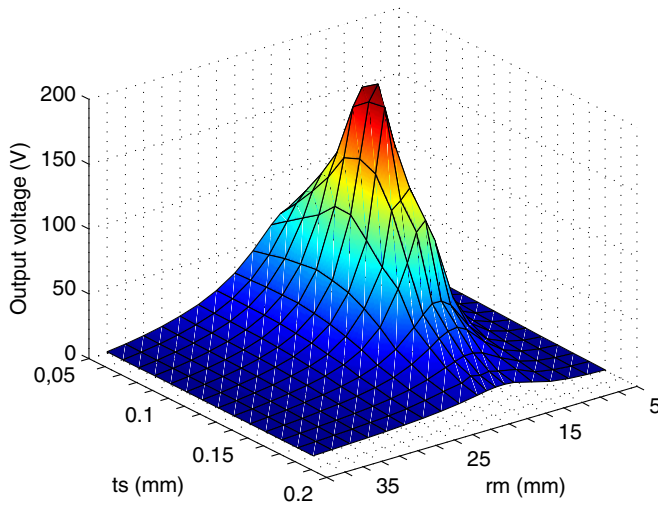

Fig. 6.   The dependence of the output voltage on the values r_m and t_s.
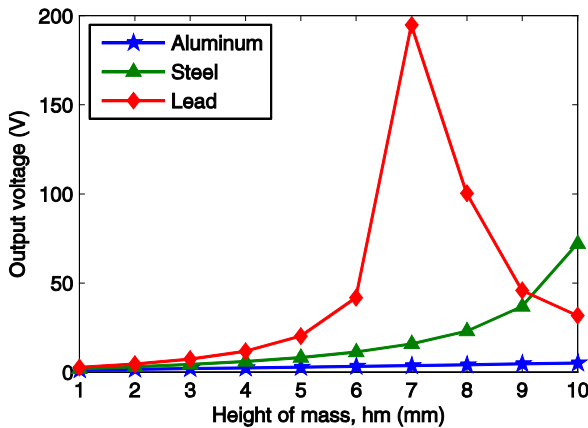

Fig. 7.   The dependence of the output voltage on the height of the proof mass h_m.

substrate plate t_s, where r_m was changing from 5 mm to 37 mm; t_s was changing from 0.05 mm to 0.18 mm; the height of the proof mass $h_m = 7$ mm and the material of the proof mass — lead.

From Fig. 6, it can be shown that when the values $r_m = 16$ mm, $t_s = 0.113$ mm, the value of the output voltage attains the maximum.

Thus, Fig. 7 shows the dependence of the output voltage on the free electrode depending on the heights of the proof mass h_m, where h_m was changing from 1 mm to 10 mm and the type of material of the proof mass (aluminum, steel or lead). The values are $r_m = 16$ mm, $r_p = 38$ mm, $t_p = 0.127$ mm, $t_s = 0.113$ mm.

From Fig. 7, it can be shown that at the value $h_m = 7$ mm, the material of the proof mass — lead, then the value of the output voltage attains the maximum.

Analysis of the results shows that the optimum parameters for a selected constraint on the dimensions of the array, the PEG has the value $r_m = 16$ mm; $r_p = 38$ mm; $t_s = 0.113$ mm; $t_p = 0.127$ mm; $h_m = 7$ mm; and the material of the proof mass — lead.

3.3.3. *Analysis on the output power of the PEG*

The analysis of output power was performed for the second harvester (Fig. 1), where power harvesters (voltage source) connect into a resistor R_l (power harvester with piezoelectric element connected in parallel). We investigate the dependence of the output voltage and power on the load increases R_l, where $t_p = 0.127$ mm, $r_p = 38$ mm, $t_s = 0.113$ mm, $r_s = 40$ mm, $h_m = 7$ mm, $r_m = 16$ mm and the material of the proof mass — lead. The results are presented in Figs. 8 and 9.

Figure 8 displays enlarged views of the voltage, the first vibration mode for these 10 different values of load resistance: 0.01, 0.1, 0.5, 1, 5, 8.7, 10, 50, 100, 1000 kohm.
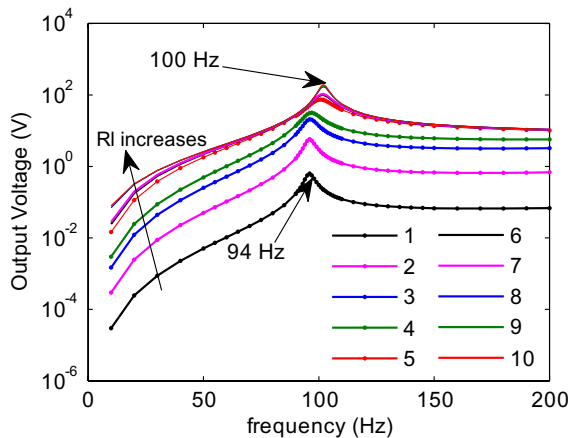

Fig. 8. Enlarged views of the voltage for 10 different values of load resistance. $1 - R_l = 0.01$ kohm, $2 - R_l = 0.1$ kohm, $3 - R_l = 0.5$ kohm, $4 - R_l = 1$ kohm, $5 - R_l = 5$ kohm, $6 - R_l = 8.7$ kohm, $7 - R_l = 10$ kohm, $8 - R_l = 50$ kohm, $9 - R_l = 100$ kohm, $10 - R_l = 1000$ kohm.
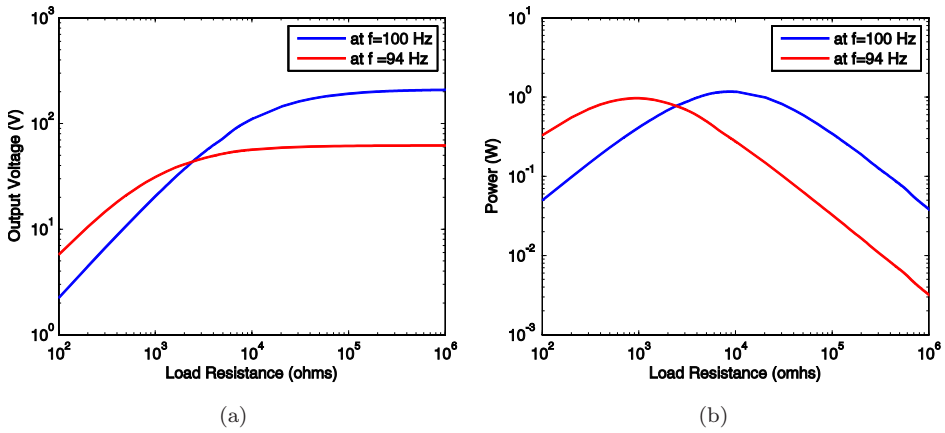
Fig. 9.   Variations of the (a) voltage output and the (b) electrical power with resistive load for excitations close to short circuit and open circuit resonance frequencies of the first vibration mode.

The direction of increasing load resistance is depicted by an arrow, and it is clear from Fig. 8 that the voltage across the resistive load increases monotonically with increasing load resistance at every excitation frequency. For the extreme values of the load resistance, the frequency of maximum voltage output moves from the short circuit resonance frequency to the open circuit resonance frequency. For a moderate value of load resistance, the frequency of maximum voltage has a value in between these two extreme frequencies (between 94 Hz and 100 Hz in this case).

Fundamental resonance frequency of the voltage response is of particular interest for the extreme cases of load resistance and this frequency is 94 Hz (for $R_l \rightarrow 0$) and 100 Hz (for $R_l \rightarrow \infty$). Variations of the voltage output with changing load resistance for excitations at these two frequencies are given in Fig. 9(a). In both cases, voltage increases monotonically with load resistance. The voltage output for excitation at the short circuit resonance frequency is higher when the system is close to short circuit conditions and vice versa. There is a certain resistive load (2.45 kohm) for which the voltage response has the same amplitude (43 volts) for excitations at both frequencies. The maximum voltage output in the limit $R_l \rightarrow \infty$ is about 60 volts for excitation at 94 Hz and it is about 195 volts for excitation at 100 Hz. Figure 9(b) shows the variations of the electrical power[1] with changing load resistance for excitations at these two frequencies. Expectedly, both cases have different optimum resistive loads which give the highest power. The optimum resistive load for excitation at 94 Hz is 0.9 kohm, yielding a maximum electrical power of about 0.9 W whereas the optimum resistive load for excitation at 100 Hz is 8.7 kohm, yielding a maximum electrical power of approximately the same value. As in the case of

---

[1]The electrical power amplitude shown in the figure is due to $P = |V|^2/R_l$; therefore, it is not the average power. The average power can be obtained from $P_{ave} = |V_{rms}|^2/R_l$, where $V_{rms} = V/\sqrt{2}$ (thus, $P_{ave} = |V|^2/2R_l = P/2$).

voltage output, the electrical power output for excitation at the short circuit resonance frequency is higher when the system is close to short circuit conditions and vice versa. Moreover, there exists a certain resistive load (2.45 kohm), which results in the same electrical power (0.8 W) for excitations at both of these frequencies.

4. Conclusions

We have studied the effectiveness of the piezoelectric energy harvesters depending on the geometric characteristics and material under certain limited conditions of the dimensions of the device. PEG was studied to convert ambient vibration energy of 100 Hz. The construction is modeled by using the FE packages ANSYS and ACELAN. A study in the FE modeling of the PEG with the use of piezoelectric ceramics and the calculation on this basis shows the limits of applicability of the simplified model taking into account the inertial mass and allows you to choose the rational dimensions of the elements to achieve maximum efficiency. In addition, this comparison of different models provides guidance to the constructor assembly technology of device, namely on the effectiveness of certain intermediate layers with low rigidity, which does not restrict the deformation of the bimorph. On the basis of calculations, it can be used for fabricating the harvesters, which works at a specified resonant frequency corresponding to the available vibrations.

References

Adhikari, S., Friswell, M. I. and Inman, D. J. [2009] "Piezoelectric energy harvesting from broadband random vibrations," *Smart Materials and Structures* **18**, 115005.

Ali, S. F. and Adhikari, S. [2013] "Energy harvesting dynamic vibration absorbers," *Journal of Applied Mechanics* **80**(4), 041004.

Amini, Y., Emdad, H. and Farid, M. [2014] "An accurate model for numerical prediction of piezoelectric energy harvesting from fluid structure interaction problems," *Smart Materials and Structures* **23**, 095034.

Anton, S. R. and Sodano, H. A. [2007] "A review of power harvesting using piezoelectric materials (2003–2006)," *Smart Materials and Structures* **16**(3), R1–R21.

Belokon, A. V., Nasedkin, A. V. and Soloviev, A. N. [2002] "New schemes for the finite-element dynamic analysis of piezoelectric devices," *Journal of Applied Mathematics and Mechanics* **66**(3), 481–490.

Berlincourt, D. A., Curran, D. R. and Jaffe, H. [1964] *Physical Acoustics. Principles and Methods* (Academic Press, Cambridge), V.1.

Boisseau, S., Despesse, G. and Seddik, D. A. [2013] "Nonlinear H-shaped springs to improve efficiency of vibration energy harvesters," *Journal of Applied Mechanics* **80**(6), 061013.

Doroushi, A., Eslami, M. R. and Komeili, A. [2011] "Vibration analysis and transient response of an FGPM beam under thermo-electro-mechanical loads using higher-order shear deformation theory," *Journal of Intelligent Material Systems and Structures* **22**(3), 231–243.

Dutoit, N. E., Wardle, B. L. and Kim, S.-G. [2005] "Design considerations for mems-scale piezoelectric mechanical vibration energy harvesters," *Integrated Ferroelectrics* **71**(1), 121–160.

Erturk, A. and Inman, D. J. [2008] "Analytical modeling of cantilevered piezoelectric energy harvesters for transverse and longitudinal base motions," *Proceedings of the 49th AIAA/ASME/ASCE/AHS/ASC Structures, Structural Dynamics, and Materials Conference*, Schaumburg, IL, 7–10 April.

Erturk, A. and Inman, D. J. [2011a] "Broadband piezoelectric power generation on high-energy orbits of the bistable Duffing oscillator with electromechanical coupling," *Journal of Sound and Vibration* **330**(10), 2339–2353.

Erturk, A. and Inman, D. J. [2011b] *Piezoelectric Energy Harvesting* (John Wiley and Sons, Ltd., New York).

Fan, K., Chang, J., Chao, F. and Pedrycz, W. [2015] "Design and development of a multipurpose piezoelectric energy harvester," *Energy Conversion and Management* **96**, 430–439.

Farnsworth, M., Tiwari, A. and Dorey, R. [2014] "Modelling, simulation and optimisation of a piezoelectric energy harvester," *Procedia CIRP* **22**, 142–147.

Gafforelli, G., Ardito, R. and Corigliano, A. [2015] "Improved one-dimensional model of piezoelectric laminates for energy harvesters including three dimensional effects," *Composite Structures* **127**, 369–381.

Jeon, Y. B., Sood, R., Jeong, J. H. and Kim, S. G. [2005] "MEMS power generator with transverse mode thin film PZT," *Sensors and Actuators A* **122**, 16–22.

Jung, H. J., Song, Y., Hong, S. K., Yang, C. H., Hwang, S. J., Jeong, S. Y. and Sung, T. H. [2015] "Design and optimization of piezoelectric impact-based micro wind energy harvester for wireless sensor network," *Sensors and Actuators A: Physical* **222**, 314–321.

Kim, H. S., Kim, J.-H. and Kim, J. [2011] "A review of piezoelectric energy harvesting based on vibration," *International Journal of Precision Engineering and Manufacturing* **12**(6), 1129–1141.

Kim, S. *et al.* [2005a] "Piezoelectric energy harvesting with a clamped circular plate: Analysis," *Journal of Intelligent Material Systems and Structures* **16**(10), 847–854.

Kim, S. *et al.* [2005b] "Piezoelectric energy harvesting with a clamped circular plate: Experimental study," *Journal of Intelligent Material Systems and Structures* **16**(10), 855–863.

Kobayashi, T., Okada, H., Masuda, T., Maeda, R. and Itoh, T. [2010] "A digital output accelerometer using mems-based piezoelectric accelerometer connected to parallel CMOS circuit," *Procedia Engineering* **5**, 1071–1074.

Lezgy-Nazargah, M., Vidal, P. and Polit, O. [2013] "An efficient finite element model for static and dynamic analyses of functionally graded piezoelectric beams," *Composite Structures* **104**, 71–84.

Liao, Y. and Sodano, A. H. [2008] "Model of a single mode energy harvester and properties for optimal power generation," *Smart Materials and Structures* **17**, 065026.

Litak, G., Friswell, M. I. and Adhikari, S. [2010] "Magnetopiezoelastic energy harvesting driven by random excitations," *Applied Physics Letters* **96**, 214103.

Mehmood, A., Abdelkefi, A., Hajj, M. R., Nayfeh, A. H., Akhtar, I. and Nuhait, A. O. [2013] "Piezoelectric energy harvesting from vortex-induced vibrations of circular cylinder," *Journal of Sound and Vibration* **332**(19), 4656–4667.

Mo, C., Leon, J. R. and Clark, W. W. [2010] "Experimental validation of energy harvesting performance for pressure-loaded piezoelectric circular diaphragms," *Smart Materials and structures* **19**(7), 75010–75016.

Monri, K. and Maruo, S. [2013] "Three-dimensional ceramic molding based on microstereolithography for the production of piezoelectric energy harvesters," *Sensors and Actuators A: Physical* **200**, 31–36.

Namli, O. C. and Taya, M. [2011] "Design of Piezo-SMA composite for thermal energy harvester under fluctuating temperature," *Journal of Applied Mechanics* **78**(3), 031001.

Priya, S. [2007] "Advances in energy harvesting using low profile piezoelectric transducers," *Journal of Electroceramics* **19**(1), 167–184.

Priya, S. and Inman, D. J. [2009] *Energy Harvesting Technologies* (Springer, New York).

Roundy, S., Leland, E. S., Baker, J., Carleton, E., Reilly, E., Lai, E., Otis, B., Rabaey, J. M., Wright, P. K. and Sundararajan, V. [2005] "Improving power output for vibration-based energy scavengers," *IEEE Pervasive Computing* **4**, 28–36.

Sodano, H. A., Park, G. and Inman, D. J. [2004a] "Estimation of electric charge output for piezoelectric energy harvesting," *Journal of Strain* **40**, 49–58.

Sodano, H. A., Park, G. and Inman, D. J. [2004b] "A review of power harvesting from vibration using piezoelectric materials," *The Shock and Vibration Digest* **36**, 197–205.

Sodano, H. A., Inman, D. J. and Park, G. [2005] "Comparison of piezoelectric energy harvesting devices for recharging batteries," *Journal of Intelligent Material Systems and Structures* **16**(10), 799–807.

Staaf, L. G. H., Köhler, E., Parthasarathy, D., Lundgren, P. and Enoksson, P. [2015] "Simulation and experimental demonstration of improved efficiency in coupled piezoelectric cantilevers by extended strain distribution," *Sensors and Actuators A: Physical* **229**, 136–140.

Stanton, S. C., Erturk, A., Mann, B. P., Dowell, E. H. and Inman, D. J. [2012] "Nonlinear nonconservative behavior and modeling of piezoelectric energy harvesters including proof mass effects," *Journal of Intelligent Material Systems and Structures* **23**(2), 183–199.

Tang, L. H., Yang, Y. W. and Soh, C. K. [2010] "Toward broadband vibration-based energy harvesting," *Journal of Intelligent Material Systems and Structures* **21**(18), 1867–1897.

Twiefel, J., Richter, B., Sattel, T. and Wallaschek, J. [2008] "Power output estimation and experimental validation for piezoelectric energy harvesting systems," *Journal of Electroceramics* **20**, 203–208.

Vatanabe, S. L., Paulino, G. H. and Silva, E. C. N. [2013] "Design of functionally graded piezocomposites using topology optimization and homogenization – Toward effective energy harvesting materials," *Computer Methods in Applied Mechanics and Engineering* **266**, 205–218.

Xie, X. D., Wang, Q. and Wu, N. [2014] "Energy harvesting from transverse ocean waves by a piezoelectric plate," *International Journal of Engineering Science* **81**, 41–48.

Zhang, C., Zhang, C. and Chen, W. [2013a] "Modeling of piezoelectric bimorph nano-actuators with surface effects," *Journal of Applied Mechanics* **80**(6), 061015.

Zhang, H., Ye, G. and Zhang, Z. [2013b] "Acoustic radiation of a cylindrical piezoelectric power transformer," *Journal of Applied Mechanics* **80**(6), 061019-061019-5.